Variable-Temperature ^{7}Li Solid-State NMR Investigation of Li-Ion Mobility and Its Correlation with Conductivity in Pore-Filling Polymer Electrolytes for Secondary Batteries

Jae-Deok Jeon and Seung-Yeop Kwak*

Hyperstructured Organic Materials Research Center (HOMRC), and School of Materials Science and Engineering, Seoul National University, San 56-1, Sillim-dong, Gwanak-gu, Seoul 151-744, Korea

Received July 7, 2006; Revised Manuscript Received August 28, 2006

ABSTRACT: We have attempted to combine a gel and a solvent-free polymer electrolyte through the concept of the pore-filling polymer electrolyte; instead of using organic solvents, a viscous poly(ethylene oxide-*co*-ethylene carbonate) (P(EO−EC)) complexed with a $LiCF_3SO_3$ is filled into the pores of a porous poly(vinylidene fluoride-*co*-hexafluoropropylene) (P(VdF−HFP))/P(EO−EC)) blend membrane. Our results indicated that the ionic conductivity of the pore-filling polymer electrolytes showing Arrhenius temperature dependence reached a maximum value of 3.7×10^{-5} S cm^{-1} at 298 K for E-V6E4, where "E-V*x*E*y*" denotes the **E**lectrolyte of P(**V**dF−HFP)/P(**E**O−EC) porous matrix (*x*/*y* by wt %) filled with the P(EO−EC)/$LiCF_3SO_3$ (in the case of E-V6E4, ca. 61 wt %). In this study, the Li-ion mobilities of a series of pore-filling E-V*x*E*y* polymer electrolytes were determined from ^{7}Li solid-state NMR line width and spin−lattice relaxation time measurements and were correlated with their ionic conductivities in conjunction with the effect and role of the amount of the P(EO−EC)/Li-salt electrolyte. In ^{7}Li NMR line width measurements, the onset temperature of ^{7}Li motional line narrowing was correlated with the glass transition temperature, T_g, of P(EO−EC) complexed with the Li-salt. Temperature dependence of correlation times, τ_c's, determined from ^{7}Li NMR line width data analysis with the Bloembergen−Purcell−Pound (BPP) theory for all polymer electrolytes, was composed of two distinctive regions above and below T_{sc} (temperature at slope change, 272−280 K), in which each region showed a linear Arrhenius behavior. In ^{7}Li NMR spin−lattice relaxation time in the rotating frame, $T_{1\rho}$, experiments, T_{max}'s (temperature at $T_{1\rho}^{-1}$ maximum, 266−276 K) of the polymer electrolytes appeared to have a trend to shift to lower temperatures with increase of the amount of the P(EO−EC)/$LiCF_3SO_3$ electrolyte, indicating that the Li-ions were more mobile. Because the temperature dependence of the $T_{1\rho}^{-1}$ exhibited maxima, the correlation times, τ_c's, were able to be calculated using the BPP equation. For the temperatures above T_{sc} and T_{max}, which were the same temperature region where ionic conductivity measurements were carried out, the correlation times, τ_c's, and the corresponding activation energies, E_a's, obtained from both ^{7}Li line width and $T_{1\rho}$ measurements decreased with increase of the amount of the P(EO−EC)/Li-salt electrolyte. From these results, it was concluded that the Li-ion mobilities of a series of pore-filling polymer electrolytes depended on the P(EO−EC)/Li-salt electrolyte content at the same temperature range from 280 to 340 K and enhanced Li-ion mobilities led to the increase of ionic conductivity, implying that Li-ion mobilities in polymer electrolytes had a strong correlation with their ionic conductivities.

1. Introduction

Solid polymer electrolytes (SPEs) formed by complexing alkali metal salts (LiX) with an ion-conducting polymer have received considerable attention, especially because of their potential applications in solid-state batteries, chemical sensors, and electrochromic devices.[1,2] These polymer electrolytes have to satisfy several requirements, including high ionic conductivity, good mechanical properties, and excellent electrochemical stability. The ionic conductivity of SPEs is due to the motion of dissolved ionic species (cations and anions) in a polymeric matrix. It is well established that conductivity occurs in the amorphous phase, above the glass transition temperature, T_g, via a liquidlike motion of the cations associated with segmental reorientations of the neighboring chains.[3] However, poly(ethylene oxide) (PEO)-based SPEs show comparatively low ionic conductivity at ambient temperature. This is due to the existence of crystalline domains that interfere with the ion transport and the dependence of the ion transport on main-chain segmental motions, which quickly diminish with decreasing temperature.[4] Thus, increasing the volume fraction of the amorphous domain in the polymer host and decreasing its T_g appear to be the main strategy to obtain better conductivity. Therefore, a variety of amorphous materials with low T_g have been developed.[5−8] Recent work has utilized various approaches to suppress the cystallinity through the incorporation of oxymethylene groups to PEO.[5,6] In addition, low T_g polyphosphazenes[7,8] and polysiloxanes[5,6] with oligoether side groups attached to the flexible backbones have been used effectively.

At present, the highest ionic conductivity of these polymer electrolytes is about 10^{-5} S cm^{-1} at room temperature, which is still lower than that of most gel polymer electrolytes (GPEs). In this respect, most of the research has focused on the preparation and characterization of GPEs which exhibit higher ionic conductivity at ambient temperature. GPEs are prepared by incorporating organic solvent electrolytes into matrix polymers, resulting in high conductivity in excess of 10^{-3} S cm^{-1} at room temperature. However, their mechanical properties are not sufficient to prepare thin films, because the impregnation of solvent electrolytes into a polar polymer results in softening of the polymer. One of the ways to solve this problem is to use a porous membrane, which plays a role of a mechanical supporter.[9−11] Even if the mechanical properties of the GPEs are improved, other properties such as solvent retention ability,

* Corresponding Author. E-mail: sykwak@snu.ac.kr. Telephone: +82-2-880-8365. Fax: +82-2-885-1748.

10.1021/ma061521v CCC: $33.50
Published on Web 10/12/2006

stability of the lithium interface, and subambient temperature conductivity should be enhanced further for practical applications.

Recently, we have attempted to combine both SPEs and GPEs through the concept of new pore-filling polymer electrolytes: instead of using organic solvents, a viscous polymer complexed with $LiCF_3SO_3$ is filled into the pores of a porous membrane, thereby producing a pore-filling polymer electrolyte.[12,13] The viscous polymer was poly(ethylene oxide-*co*-ethylene carbonate) copolymer (P(EO−EC)), with a low number-average molecular weight of about 1800 g mol^{-1}, which was synthesized using ethylene carbonate (EC). From the beginning of the reaction, CO_2 gas was evolved from the reaction mixture, which resulted in formation of ethylene oxide units, so that P(EO−EC) copolymer consisting of ca. 70 mol % of ethylene oxide units and ca. 30 mol % of ethylene carbonate units was synthesized. Because of the high polarity of carbonate groups linked by ether moieties, the dielectric constant of the P(EO−EC) should be higher than that of pure polyether-based systems, and the free ion content of the salt-in-polymer electrolyte should be higher.[14] This polymer with a high dielectric constant should reduce ion clustering with an attendant increased conductivity.[15] In addition, an interesting feature of the P(EO−EC) is its lack of crystallinity. Therefore, the amorphous nature of the P(EO−EC) allows this material to be successfully used as an ion-conducting polymer electrolyte with no detrimental effects by crystallization.

^{7}Li solid-state NMR has emerged as one of the highly sophisticated techniques to obtain the information about the mobility of the charge carriers and also to gain insight into the salt−polymer interactions in the polymer electrolytes.[16−18] This technique is also highly sensitive to the dynamics of Li-ion and polymer chain based on the effects that such motions have on the nuclear spin-relaxation times. Therefore, measurements of these relaxation times as a function of temperature are used to study the correlation between the Li-ion and polymer chain segmental motion in pore-filling polymer electrolytes having different P(EO−EC)/Li−salt contents. In the present paper, we report ^{7}Li solid-state NMR study as a function of temperature in a series of polymer electrolytes containing various electrolyte contents and its correlation with ionic conductivity. ^{7}Li solid-state NMR is used to study the motion of the mobile cation through the measurements of line widths, $\Delta\nu$, and spin−lattice relaxation times in the laboratory frame, T_1, and in the rotating frame, $T_{1\rho}$. These data are compared with those deduced from conductivity measurements.

2. Experimental Section

2.1. Materials. Acetone (Aldrich Chemicals), ethylene glycol (Aldrich Chemicals), and methanol (Daejung Chemicals & Metals (Korea)) were used as received. Lithium trifluoromethane sulfonate ($LiCF_3SO_3$, Aldrich Chemicals) was used as an electrolyte salt for the polymer electrolytes. $LiCF_3SO_3$ was dried under high vacuum prior to use. Poly(vinylidene fluoride-*co*-hexafluoropropylene) (P(VdF−HFP), $M_w = 4.6 \times 10^5$ g mol^{-1}) was purchased from Aldrich Chemicals. The P(EO−EC) ($M_n = 1800$ g mol^{-1}) was synthesized by a ring-opening polymerization of EC in the presence of potassium methoxide (CH_3OK) as an initiator. The synthesis procedure of P(EO−EC) has been described in detail in our previous report.[12]

2.2. Preparation of Polymer Electrolytes. Porous membranes to mechanically support the pore-filling polymer electrolyte were obtained by the phase inversion technique, as described elsewhere.[9,19] Briefly, P(VdF−HFP) and P(EO−EC) were dissolved in a mixture of acetone (a solvent) and ethylene glycol (a nonsolvent) such that the amount of the nonsolvent was low enough to allow solubilization and high enough to allow phase inversion upon evaporation. The composition of polymers was $(10 - x)$ wt % P(VdF−HFP)/x wt % P(EO−EC), where $x = 0$, 2, and 4. The weight ratio of polymers, a solvent, and a nonsolvent was 1:8:1. The resulting solution was cast as a film on a glass substrate, and the solvent was allowed to evaporate at ambient temperature. Then the nonsolvent was removed by washing with methanol. The prepared porous membranes were kept under vacuum for 24 h at 323 K to completely remove the traces of a solvent and a nonsolvent.

To prepare a viscous electrolyte, P(EO−EC) was first dissolved in acetone. When completely homogeneous solution was obtained, an appropriate amount of $LiCF_3SO_3$ was added and then was further stirred until the Li-salt was completely dissolved. The resulting solution was left to evaporate the solvent under vacuum at ambient temperature. After complete removal of the solvent, the heated viscous electrolyte was filled into the pores of a porous membrane by using vacuum filter equipment, thereby producing a pore-filling polymer electrolyte. The electrolyte remaining on the surface was wiped with a filter paper. All of the experiments were performed in a dry room.

In this study, M-VxEy and E-VxEy shall denote the porous **M**embrane with composition of P(**V**dF−HFP)/P(**E**O−EC) (x/y wt %) and the polymer **E**lectrolyte filled with the P(EO−EC)/Li-salt mixture inside the pores of its membrane, respectively.

2.3. ^{1}H Solid-State NMR. To determine the miscibility between P(VdF−HFP) and P(EO−EC) for porous membranes, the proton spin−lattice relaxation time, T_1, measurements were performed with a Bruker mq20 Minispec system with proton resonance frequency of 20 MHz at 303 K for porous membranes. Inversion−recovery (i.e., 180°−τ−90°) sequences with 2 μs 90° pulse width, 1 ms dead time, 40 scans, and 0.3 s recycle delay time was employed to determine the T_1.

2.4. Differential Scanning Calorimetry (DSC). DSC measurements were performed on two samples with a scan rate of 10 K min^{-1} from 203 to 373 K under nitrogen atmosphere using a TA Instruments model 2920 apparatus.

2.5. Ionic Conductivity. The electrical properties of the samples were analyzed by complex impedance spectroscopy between 278 and 368 K with a Zahner Electrik IM6 apparatus in the frequency range of 0.1 Hz to 1 MHz and an applied voltage of 5 mV. The samples for the measurements were prepared by sandwiching the polymer electrolyte between two stainless steel (SS) electrodes. Each sample was allowed to equilibrate for 30 min at each temperature prior to taking measurements. The ionic conductivity, σ, was then calculated from the electrolyte resistance, R_b, obtained from the intercept of the real axis of an impedance spectrum, the electrolyte thickness, l, and the electrode area, A, using the equation $\sigma = l/AR_b$.

2.6. ^{7}Li Solid-State NMR. ^{7}Li ($I = {}^3/_2$) solid-state NMR experiments were performed as a function of temperature with the purpose of determining the Li-ion mobilities of a series of pore-filling E-VxEy polymer electrolytes. For NMR measurements, the polymer electrolyte samples were transferred into 5 mm o.d. Pyrex tubes in a glovebox under dry nitrogen and sealed under reduced pressure. NMR spectra were recorded using a modified Bruker CXP 300 spectrometer operating at a ^{7}Li resonance frequency of 155.4 MHz and were successively acquired with and without ^{1}H decoupling. The line widths were taken to be the full width at half-maximum (fwhm) of the peaks and measured as a function of temperature from 230 to 340 K. ^{7}Li spin−lattice relaxation times in the laboratory frame, T_1's, were measured by inversion−recovery (i.e., 180°−τ−90°) sequences in the temperature range of 240−370 K. ^{7}Li spin−lattice relaxation times in the rotating frame, $T_{1\rho}$'s, in the temperature of 240−340 K for polymer electrolytes, were measured by a spin−lock−delay τ pulse sequence. Because of the high sensitivity for ^{7}Li NMR measurements, the uncertainties in the obtained values for ^{7}Li line widths and spin−lattice relaxation times were approximately 5%.

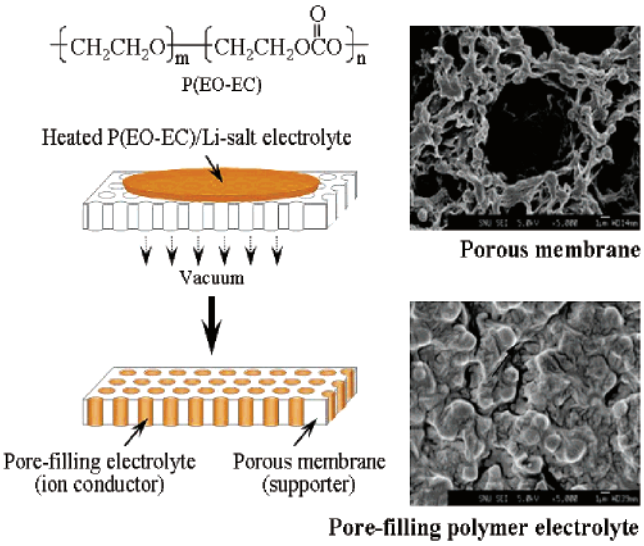

Figure 1. Concept of the pore-filling polymer electrolyte based on a porous membrane filled with a viscous polymer/Li-salt electrolyte. (a) and (b) show typical FE-SEM micrographs of a porous membrane (M-V6E4) and a polymer electrolyte (E-V6E4), respectively. P(EO−EC) is used as a viscous polymer; it comprises *m* and *n* units of ethylene oxide and ethylene carbonate, equal to 21 and 9, respectively.

Table 1. Characteristic Data of the Porous Membranes and Polymer Electrolytes

porous membranes				polymer electrolytes	
sample	porosity[a]	T_1 (s)	domain size, $\langle L \rangle$ (nm)	sample	uptake[b]
M-V10E0	54.3	0.78	21.6	E-V10E0	36.4
M-V8E2	59.1	0.42	15.9	E-V8E2	48.2
M-V6E4	64.6	0.35	14.5	E-V6E4	61.3

[a] Determined as $(W_a/\rho_a)/((W_a/\rho_a + W_p/\rho_p)) \times 100$, where W_a is the weight of the wet (filled with *n*-butanol) membrane, W_p the weight of the dry membrane, ρ_a the density of *n*-butanol, and ρ_p the density of the membrane. [b] Determined as $(W_a - W_p)/W_a \times 100$, where W_a and W_p are the weights of the wet (filled with a viscous P(EO−EC)/Li-salt electrolyte) and dry membranes, respectively.

3. Results and Discussion

3.1. ^{1}H NMR Spin−Lattice Relaxation. Our strategy in the development of SPEs for rechargeable lithium batteries involves filling a viscous polymer instead of conventional organic solvents inside the pores of a porous membrane, as shown in Figure 1. The porous membrane and the viscous P(EO−EC)/Li-salt electrolyte play effective roles as a supporter and an ion conductor, respectively. Figure 1b shows that a viscous polymer is well filled inside the pores of a porous membrane (Figure 1a), thereby producing a solvent-free pore-filling polymer electrolyte. Porous membranes prepared by a phase inversion method were composed of two materials: P(VdF−HFP), with excellent mechanical properties, and P(EO−EC), with good flexible properties. The existence of viscous P(EO−EC) in membranes contributed to an increase in the porosity, which could reach up to 65% depending on P(EO−EC) composition, thereby resulting in high uptake and ionic conductivity. These results are listed in Table 1. To evaluate the miscibility of P(VdF−HFP) and P(EO−EC), porous membranes were characterized using differential scanning calorimetry (DSC). For a series of M-V*x*E*y* porous membranes, however, it was difficult to detect their intermediate T_g values due to the semicrystallinity of P(VdF−HFP). It was reported that the intermediate T_g for the P(VdF−HFP)/polyacrylonitrile (PAN) blend membrane could not be observed because P(VdF−HFP) is a semicrystalline.[10]

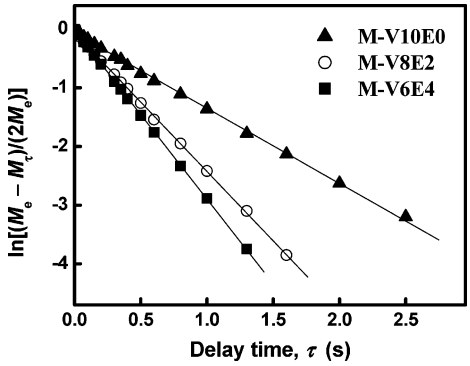

Figure 2. Logarithmic plots of resonance intensity vs delay time for porous membranes. The slope yields the proton spin−lattice relaxation time in the laboratory frame, T_1.

In this study, to best determine the miscibility of P(VdF−HFP)/P(EO−EC)-based porous membranes, T_1's were measured using ^{1}H solid-state NMR. According to the 180°−τ−90° inversion−recovery scheme, a single T_1 relaxation complies with the following condition

$$\ln[(M_e - M_\tau)/(2M_e)] = -\tau/T_1 \quad (1)$$

where M_τ and M_e are the intensities of the resonance at a given delay time, τ, and equilibrium state ($\tau \geq 5T_1$), respectively. By plotting of $\ln[(M_e - M_\tau)/(2M_e)]$ against τ, straight lines with different slopes were obtained corresponding to the pure and blend membranes, indicating a single component T_1 relaxation behavior (Figure 2). From the slopes of the plots, T_1 values were obtained. The results are summarized in Table 1. The fact that a single T_1 was observed indicates that the spin diffusion process is sufficiently fast to equilibrate the relaxation times for all protons among the chemically different constituents and blend membranes are completely homogeneous on the time scale of the T_1.

T_1 relaxation experiments also provide an estimate of the diffusive path length and hence the sizes of blend heterogeneities. A useful approximation of the upper limit to the domain size can be calculated by the following equation

$$\langle L \rangle = (6DT)^{1/2} \quad (2)$$

where $\langle L \rangle$ is the average diffusive path length for the effective spin diffusion, and D is the effective spin diffusion coefficient determined by the average proton−proton distance and the strength of the dipolar interaction. A typical value of D for an ordinary polymer is of the order of 10^{-16} m^2 s^{-1}. T is the relaxation time, T_1 or $T_{1\rho}$, according to the type of relaxation measurements, and has the T_1 value in this study. Using eq 2 and considering the T_1 values of porous membranes, the average diffusive path length, viz. domain size of the M-V8E2 and M-V6E4, was calculated to be about 14−16 nm, and thus it was concluded that two components (i.e., P(VdF−HFP) and P(EO−EC)) in the blend were uniformly mixed on the scale of a few tens of nanometers.

3.2. DSC and Ionic Conductivity. Typical DSC traces for viscous P(EO−EC)s with and without Li-salt are shown in Figure 3. The neat P(EO−EC) was in the amorphous state because no melting transition was observed in the thermograms. When the salt was added, the T_g increased markedly, i.e., from 229 to 246 K, via the so-called "salt effect". The increase in T_g can be attributed to ion−dipole interactions reducing the segmental motion of the P(EO−EC), which in turn affects the flexibility of the chains. This behavior is similar to most of

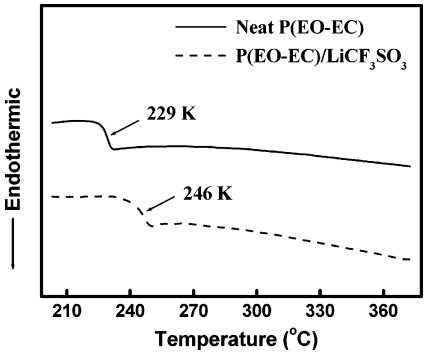

Figure 3. Typical DSC trace for films with 1.5 mmol-$LiCF_3SO_3$/g-P(EO−EC) and without Li-salt.

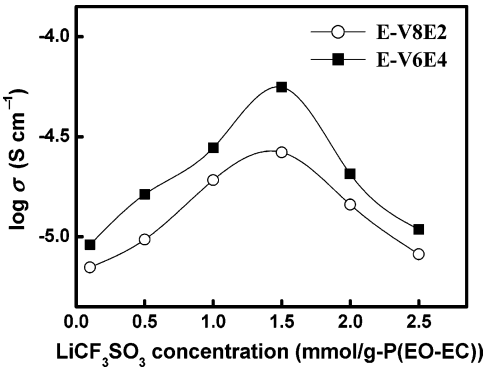

Figure 4. Salt concentration dependence of ionic conductivity for polymer electrolytes.

polymer electrolytes formed by complexes of a Li-salt with a polyether-based polymer.

Figure 4 shows the salt concentration dependence of the conductivity and the lithium salt concentration from *x*-mmol $LiCF_3SO_3$/g-P(EO−EC) ($x = 0.1-2.5$) for the E-V8E2 and E-V6E4 at 303 K. At 1.5-mmol $LiCF_3SO_3$/g-P(EO−EC), the conductivity reaches its maximum, 2.6×10^{-5} S cm^{-1} for an E-V8E2 sample and 5.6×10^{-5} S cm^{-1} for an E-V6E4 sample. The conductivity, σ, of polymer electrolytes increased with increasing the salt concentration up to 1.5-mmol $LiCF_3SO_3$/g-P(EO−EC), but further addition of the salt caused the decrease of the conductivity. Conductivity is related to the number of charge carriers, n_i, and their mobility, μ_i, according to the following equation[20]

$$\sigma = \sum_i n_i q_i u_i \tag{3}$$

where q_i is the charge on each charge carrier. Therefore, below salt concentration of 1.5-mmol $LiCF_3SO_3$/g-P(EO−EC), it appears that the increase in the number of charge carriers is responsible for the increase in the conductivity for both polymer electrolytes. However, at higher salt concentration, the conductivity decreases due to the increasing influence of ion pairs, triplets, and higher ion aggregations, which reduces the overall mobility and the number of effective charge carriers. Consequently, the optimum salt concentration was 1.5-mmol $LiCF_3SO_3$/g-P(EO−EC) and used throughout the subsequent series of measurements.

Figure 5 shows the temperature dependence of the conductivity for polymer electrolytes. It was confirmed that the conductivity of polymer electrolytes increased with the increase of the P(EO−EC)/$LiCF_3SO_3$ content (i.e., E-V6E4 > E-V8E2 > E-V10E0). This is related to the enhanced ion mobility and the increased number of charge carriers. This ion mobility will be

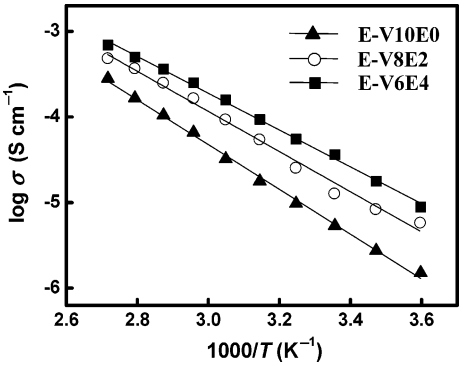

Figure 5. Temperature dependence of ionic conductivity for polymer electrolytes. Data are fitted using the Arrhenius equation (solid lines).

Table 2. Results Obtained from Regressing Arrhenius Equation onto the Conductivity Data for the Polymer Electrolytes

sample	σ (S cm^{-1}) at 298 K	log σ_o (S cm^{-1})	E_a (kJ mol^{-1})
E-V10E0	5.4×10^{-6}	3.52 ± 0.1	50.1 ± 0.8
E-V8E2	1.3×10^{-5}	3.15 ± 0.2	45.2 ± 1.2
E-V6E4	3.7×10^{-5}	2.72 ± 0.1	41.2 ± 0.7

discussed below. The E-V6E4 with the highest P(EO−EC)/$LiCF_3SO_3$ electrolyte content showed a maximum conductivity value of 3.7×10^{-5} S cm^{-1} at 298 K. This is still lower than that of most gel system electrolytes, but nonetheless, it is noteworthy in itself that the value is higher than that for the $LiCF_3SO_3$−poly[oligo(ethylene glycol)-oxalate] complex[14] of ca. 8.0×10^{-7} S cm^{-1} at 298 K and $LiCF_3SO_3$−poly(methoxytriethyleneoxide)methylsiloxane complex[21] of ca. 1.2×10^{-5} S cm^{-1} at 303 K, which are the solvent-free system electrolytes based on an amorphous polymer of a low molecular weight. This difference in conductivity is due to the pore-filling system prepared by filling the pores with a P(EO−EC)/$LiCF_3SO_3$ electrolyte, which plays an effective role of an ion conductor. Interestingly, even though there was a slight curvature in some of the plots, all of the polymer electrolytes showed a linear enhancement of the conductivity when the temperature was increased, but much less than that observed in similar plots for conventional SPEs. This means that the ion conduction mechanism of these polymer electrolyte systems was not due to the dynamic configuration of the polymer matrix but rather due to the conduction path that was formed by filling the pores of porous membranes with a viscous electrolyte.[22]

On the other hand, ionic conductivity increased with increasing temperature. This temperature dependence of the ionic conductivity, σ, is well described by the Arrhenius equation

$$\sigma = \sigma_o \exp(-E_a/RT) \tag{4}$$

where T is temperature on the Kelvin scale, σ_o is a preexponential factor proportional to the number of carrier ions, R is the ideal gas constant, and E_a is the activation energy. The parameter values determined from regressing eq 4 are given Table 2. E_a values decreased with increase of the amount of the P(EO−EC)/Li-salt electrolyte, giving a lowered temperature dependence of the conductivity. It is noteworthy that the polymer electrolytes with high P(EO−EC)/Li-salt electrolyte content can have the advantages of low temperature dependence and consequent uniform response over a wide temperature range in practical applications.

3.3. ^{7}Li NMR Line Width. It is important to study the motion of the mobile Li-ion in polymer electrolytes because the Li-ions move in a dynamic environment created by the polymer motion in amorphous phase and their transport is correlated to

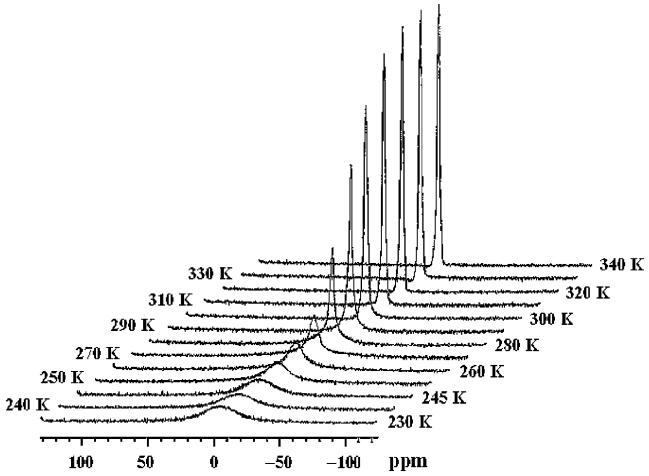

Figure 6. Temperature dependence of the ^{7}Li NMR spectra for E-V6E4 with 1.5 mmol-$LiCF_3SO_3$/g-P(EO−EC) at temperatures as shown in the plot.

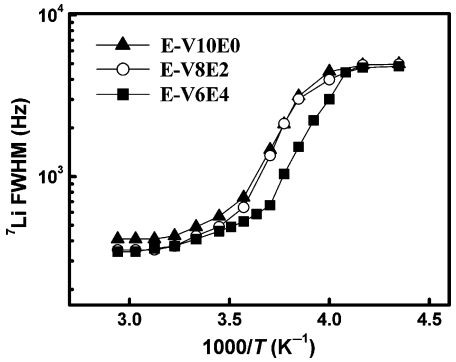

Figure 7. Line widths of ^{7}Li NMR spectra for polymer electrolytes as a function of temperature. The uncertainties in the ^{7}Li line widths are approximately 5%.

the ionic conductivity. The Li-ion mobility was investigated by measuring the line width of the central ^{7}Li transition as a function of P(EO−EC)/$LiCF_3SO_3$ electrolyte content as well as temperature. Below the T_g, the ^{7}Li spectra consist of a very intense central transition ($^1/_2 \leftrightarrow -^1/_2$) and an almost unobservably weak and broad line that could be associated with the quadrupolar satellite transitions ($^3/_2 \leftrightarrow {}^1/_2$ and $-^1/_2 \leftrightarrow -^3/_2$). Above the T_g, the weak and broad line associated with the quadrupolar satellite peaks is averaged out as the temperature is raised from T_g. That is, for nuclear spins $I > {}^1/_2$ with small quadrupolar moment such as ^{7}Li, the central transition line width is primarily determined by dipole−dipole interactions.[23−25] For this reason, only the ^{7}Li central transition was analyzed in this study. A significant reduction in the ^{7}Li line width was achieved by the use of the high-power ^{1}H decoupling technique, which effectively removed the ^{1}H−^{7}Li dipolar interactions of lithium cation and P(EO−EC) backbone. Figure 6 shows the temperature dependence of the ^{7}Li central transition ($^1/_2 \leftrightarrow -^1/_2$) line widths of E-V6E4 filled with ca. 61 wt % of the P(EO−EC)/$LiCF_3SO_3$ electrolyte. Similar NMR lines were observed for all the samples. Figure 7 shows the ^{7}Li central transition line widths as a function of temperature for the three polymer electrolytes. Below the T_g (ca. 246 K) of the P(EO−EC)/$LiCF_3SO_3$ electrolyte, the line widths are very broad and are approaching the rigid lattice line width. This suggests that the Li-ions are essentially immobile and therefore the line width is the result of increased quadrupolar or internuclear dipole−dipole interactions. As the temperature increases, the line widths are gradually narrowed, with the onset of narrowing related to the

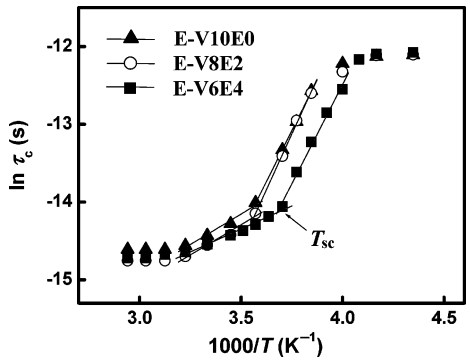

Figure 8. Temperature dependence of the corresponding correlation time, τ_c, calculated from the ^{7}Li NMR line width data by using the BPP equation for polymer electrolytes.

T_g of P(EO−EC) complexed with the Li-salt. Thus, the Li-ions are mobile near the onset temperature of Li-ion motional narrowing, which is in very good accordance with T_g measured by DSC experiments. The line widths also reach the high-temperature limit due to magnetic field inhomogeneties. On the other hand, the line width for E-V6E4 was smaller as compared to the other samples over the temperature range investigated, suggesting its higher Li-ion mobility that correlates with its higher conductivity.

The NMR motional narrowing of the line width takes place when the rate of fluctuations of the local magnetic fields or electric field gradients, which are generally described by a correlation time, τ_c, is of the order of the rigid lattice line width, $\delta\omega_o$

$$1/\tau_c \cong \delta\omega_o \tag{5}$$

The τ_c is given during the narrowing process by the Bloembergen−Purcell−Pound (BPP) theory and the following equation[26]

$$(\Delta\nu)^2 = \left(\frac{2}{\pi}\right)\delta\omega_o{}^2 \tan^{-1}(\tau_c\Delta\nu) \tag{6}$$

where $\Delta\nu$ is the measured line width, fwhm at a given temperature. For all of the samples, the onset of the rigid lattice line width (ca. 4.5−5 kHz) occurs at about T_g of the P(EO−EC)/$LiCF_3SO_3$ mixture inside the pores of a porous membrane. The temperature dependence of the τ_c is assumed to follow Arrhenius behavior, for which the activation energy, E_a, for the Li-ion mobility is determined

$$\tau_c = \tau_o \exp(E_a/RT) \tag{7}$$

Taking the natural logarithm of both sides, eq 7 gives

$$\ln \tau_c = \frac{E_a}{kT} + \ln \tau_o \tag{8}$$

where τ_o is the prefactor (or dwell time), which has the meaning of a reciprocal frequency attempt for cations jumps. When the ln τ_c is plotted as a function of inverse temperature, T^{-1}, and fit to eq 8, it yields the mean τ_o and E_a. Figure 8 shows the temperature dependence of ln τ_c obtained from the line width data except both the lowest and highest temperature limits corresponding to the rigid lattice line width and magnetic field inhomogeneities, respectively. Interestingly, the plots for all polymer electrolytes are composed of two different regions separated by a low- and a high-temperature range at ca. 272−280 K (denote hereafter as T_{sc}, temperature at slope change)

Table 3. Parameters Obtained from ^{7}Li NMR Line Width Measurements for Polymer Electrolytes

sample	T_{sc} (K)	τ_o (10^{-9} s), above T_{sc}	τ_o (10^{-15} s), below T_{sc}	E_a (kJ mol^{-1}) above T_{sc}	E_a (kJ mol^{-1}) below T_{sc}
E-V10E0	280	2.9 ± 0.9	5.4 ± 1.8	13.1 ± 0.7	43.4 ± 0.4
E-V8E2	278	2.6 ± 1.1	1.0 ± 0.4	12.9 ± 0.6	47.4 ± 0.8
E-V6E4	272	9.3 ± 1.9	5.2 ± 1.5	9.8 ± 0.5	42.4 ± 1.1

and each plot shows a linear type (Arrhenius) of behavior. It means that there is an abrupt decrease of ion mobility with decreasing temperature near T_{sc}, corresponding to the rapid change in the slope of the τ_c. For the temperatures above T_{sc}, which was the same temperature region where ionic conductivity measurements were carried out, correlation times and activation energies were gradually decreased with increase of the amount of the P(EO−EC)/$LiCF_3SO_3$ electrolyte. This result is well coincident with Arrhenius behavior from conductivity experiments in the same temperature range. The activation energies in a high-temperature region (above T_{sc}) are approximately five times larger than those in a low-temperature region (below T_{sc}). Therefore, it is very noteworthy to determine T_{sc} related to the sudden deterioration of characteristic parameters (e.g., correlation time, activation energy, and ionic conductivity). These activation energies (above T_{sc}) are comparable to those of other polymer electrolytes such as poly(vinyl alcohol)/$LiCF_3SO_3$-based SPEs (ca. 19−24 kJ mol^{-1})[20] and polyurethane/poly(dimethylsiloxane)/$LiClO_4$-based SPEs (ca. 13−19 kJ mol^{-1}).[25] In addition, in the same temperature range, activation energies from the analysis of the conductivity data corresponding to the energy barrier of Li-ion motion are approximately twice larger than those from ^{7}Li NMR data. Bishop and Bray[27] have also observed differences in NMR and conductivity activation energies in lithium borate glasses because the ^{7}Li NMR and conductivity can detect ion motions on a local scale and a more global scale, respectively. That is, the energy barrier for the Li-ion to exceed in order to undergo global motions is higher than that of local motions. Table 3 summarizes the parameters obtained from ^{7}Li line width data for the three samples investigated.

3.4. ^{7}Li NMR Spin−Lattice Relaxation. In general, in the case of quadrupolar nucleus ^{7}Li ($I = 3/2$), the spin−lattice relaxation should be described by a distribution of two or more exponential functions.[28] Becasuse of the small quadrupole moment of ^{7}Li, however, deviations from a single-exponential function are often hard to detect,[23−25] as was also found in this study. Therefore, for all samples and temperatures, the ^{7}Li T_1 and $T_{1\rho}$ data were calculated using only one exponential function. ^{7}Li spin−lattice relaxation time measurements were performed to analyze the Li-ion transport behavior. Figure 9 (see the lower graphs) shows the temperature dependence of the ^{7}Li spin−lattice relaxation rates in the laboratory frame, T_1^{-1}, of the polymer electrolytes. Above 240 K, T_1^{-1} increased drastically with increasing temperature up to a maximum value of ca. 3 s^{-1} at $T \geq 360$ K in all of the polymer electrolytes investigated, suggesting that the Li-ions become less and less mobile. The E-V6E4 displayed well-defined T_1^{-1} maximum at 360 K, which was an indication that only one process of motion of the Li-ions was taking place. In the case of E-V10E0 and E-V8E2, however, T_1^{-1} maxima were not observed in the investigated temperature range. To gain better understanding of the Li-ion mobility in polymer electrolytes, ^{7}Li spin−lattice relaxation time in the rotating frame, $T_{1\rho}$ measurements were measured in the temperature range of 240−340 K.

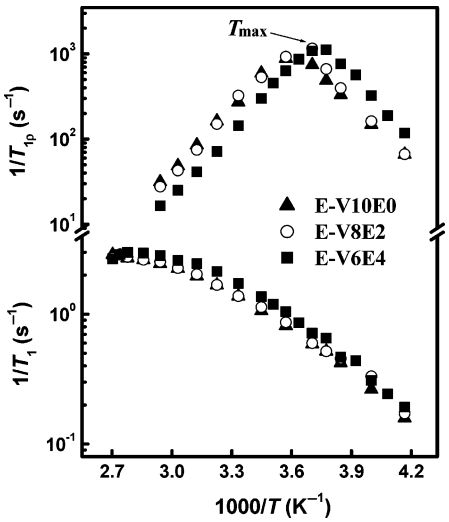

Figure 9. Temperature dependence of the ^{7}Li spin−lattice relaxation rates, T_1^{-1} and $T_{1\rho}^{-1}$, for polymer electrolytes measured at the Larmor frequency 155.4 MHz. The uncertainties in the ^{7}Li spin−lattice relaxation rates are approximately 5%.

Figure 9 (see the upper graphs) displays the Arrhenius plots of the ^{7}Li $T_{1\rho}^{-1}$ for the polymer electrolytes. In all cases of polymer electrolytes, $T_{1\rho}^{-1}$ plots versus reciprocal temperature exhibited maxima, which indicated the most efficient relaxation; the $T_{1\rho}^{-1}$ located in the left side of the maximum imply the fast motion, and vice versa. The $T_{1\rho}^{-1}$ maxima (also called T_{max}) of the polymer electrolytes appeared to have a trend to shift to lower temperatures with increase of the amount of the P(EO−EC)/$LiCF_3SO_3$ electrolyte, indicating that the Li-ions were more mobile. This can be correlated with the increased conductivity observed for these polymer electrolytes. It is therefore noteworthy that even the same value of $T_{1\rho}^{-1}$ may be in very different motional states, depending on whether they are located on the slow side or the fast side of the maximum. Thus, to avoid such confusion and to relate $T_{1\rho}$'s to molecular mobility, it is necessary to determine the correlation time, τ_c, for which quantitative analyses by BPP/KT[26,29] theory provide the relationship between the relation rate, internuclear distance, resonance frequency, and spectral density function of molecular motion (i.e., a measure of relative amount of motion). For lithium, the principal mechanism of relaxation is through the time-dependent dipolar interaction, and the relaxation rates are given by

$$\frac{1}{T_{1\rho}} = \frac{3}{2}\gamma^4\hbar^2 I(I+1)\left[\frac{1}{4}J(2\omega_1) + \frac{5}{2}J(\omega_0) + \frac{1}{4}J(2\omega_0)\right] \quad (9)$$

where γ is the lithium magnetogyric ratio, $\hbar$ is Planck's constant divided by 2π, r is the distance between coupled spins, I is the spin quantum number ($= 3/2$), $J(\omega)$ is the spectral density function at particular frequency, ω_1 is spin-lock filed frequency, and ω_0 is the Larmor frequency. Because $J(\omega)$ is given by

$$J(2\omega_1) = \frac{24}{15r^6}\left[\frac{\tau_c}{1 + 4\omega_1^2\tau_c^2}\right] \quad (10)$$

$$J(\omega_0) = \frac{4}{15r^6}\left[\frac{\tau_c}{1 + \omega_0^2\tau_c^2}\right] \quad (11)$$

$$J(2\omega_0) = \frac{16}{15r^6}\left[\frac{\tau_c}{1 + 4\omega_0^2\tau_c^2}\right] \quad (12)$$

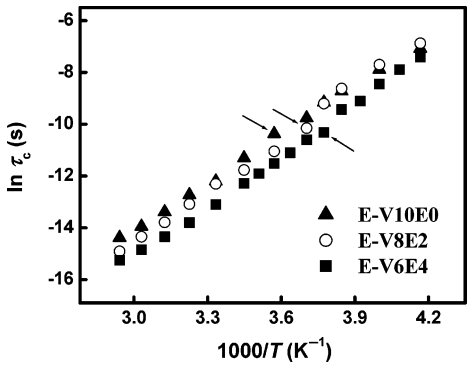

Figure 10. Temperature dependence of the correlation times calculated from the ^{7}Li NMR $T_{1\rho}$ data by using the BPP equation for polymer electrolytes. The arrows represent the temperature at $T_{1\rho}^{-1}$ maximum, T_{max}.

Table 4. Parameters Obtained from ^{7}Li NMR $T_{1\rho}$ Measurements for Polymer Electrolytes

		τ_o (10^{-15} s)		E_a (kJ mol^{-1})	
sample	T_{max} (K)	above T_{max}	below T_{max}	above T_{max}	below T_{max}
E-V10E0	276	4.2 ± 0.4	54.3 ± 8.6	52.6 ± 0.6	47.0 ± 1.3
E-V8E2	270	3.9 ± 0.6	28.8 ± 5.5	51.6 ± 0.4	48.6 ± 1.8
E-V6E4	266	2.9 ± 0.3	0.8 ± 0.2	51.1 ± 0.5	54.6 ± 1.5

the relation between relaxation and Li-ion motion is established as

$$\frac{1}{T_{1\rho}} = \frac{3}{2r^6}\gamma^4\hbar^2\left[\frac{2.5\tau_c}{1+\omega_0^2\tau_c^2} + \frac{\tau_c}{1+4\omega_0^2\tau_c^2} + \frac{1.5\tau_c}{1+4\omega_1^2\tau_c^2}\right] \quad (13)$$

With this relation, τ_c values can be extracted by nonlinear curve fitting of $T_{1\rho}$ data at the corresponding temperature. The τ_c values for the polymer electrolytes are shown as a function of inverse temperature in Figure 10. To compare the results measured at the same temperature range as that in which ionic conductivity measurements were carried out, the plots for all polymer electrolytes were separated by two different regions (i.e., above and below T_{max}), in which each region showed a linear Arrhenius behavior. For the temperatures above T_{max}, which was the same temperature region where ionic conductivity measurements were carried out, the τ_c values of polymer electrolytes decreased in the sequence of E-V10E0, E-V8E2, and E-V6E4. This ordering in τ_c values is in good agreement with the trend in ionic conductivity values measured in the temperature range of 278−368 K, indicating the higher mobility as the P(EO−EC)/$LiCF_3SO_3$ content increased. Below T_{max}, however, the τ_c value of E-V10E0 showed higher than that of E-V8E2.

Further insight into the Li-ion motion is to determine the activation energy, E_a, which corresponds to the barrier height for the potential hindered motion. It has been well-known that the temperature dependence of the correlation time for polymer electrolytes follows an Arrhenius expression as eq 7. Table 4 shows E_a values calculated from the low- and high-temperature slopes of the relaxation curves. In the case of E_a values in the high-temperature range (above T_{max}), they decreased with increase of the amount of the P(EO−EC)/$LiCF_3SO_3$ electrolyte, exhibiting a weaker temperature dependence of correlation time. This behavior is consistent with the changes in E_a values calculated from ionic conductivity and line width data. Thus, we presume that the increase of the amount of the P(EO−EC)/$LiCF_3SO_3$ electrolyte contributes to enhancement in the Li-ion mobility as well as increase in the number of charge carriers, thereby resulting in increase of ionic conductivity. Therefore, this is of critical importance in determining the conductivity of the polymer electrolyte because it affects the number of charge carriers and Li-ion mobility.

4. Conclusions

Pore-filling polymer electrolytes were prepared by filling viscous P(EO−EC)/$LiCF_3SO_3$ electrolytes into the pores of porous membranes. Porous membranes consisting of P(VdF−HFP) and P(EO−EC) were prepared by a phase inversion method and their miscibility was investigated by using ^{1}H solid-state NMR. Results indicated that they were homogeneous on a scale of a few tens of nanometers. The conductivity of polymer electrolytes with Arrhenius temperature dependence increased with increase of the amount of the P(EO−EC)/$LiCF_3SO_3$ electrolyte and reached the maximum value of 3.7×10^{-5} S cm^{-1} at 298 K for E-V6E4. In ^{7}Li NMR line width measurements, the Arrhenius plots of the correlation time, τ_c, were composed of two distinctive regions about 272−280 K (temperature at slope change, T_{sc}) for all polymer electrolytes. For the temperatures above T_{sc}, which was the same temperature region where ionic conductivity measurements were carried out, Arrhenius plots of correlation times, τ_c's, obeyed Arrhenius behavior, which was in good agreement with results observed from ionic conductivity data and their correlation times and activation energies decreased with increase of the amount of the P(EO−EC)/Li-alt electrolyte. In ^{7}Li NMR $T_{1\rho}$ measurements, well-defined $T_{1\rho}^{-1}$ maxima (also called T_{max}) of the all polymer electrolytes were observed, which suggests that only one process of Li-ion motion is taking place. T_{max} values of the polymer electrolytes appeared to have a trend to shift to lower temperatures with increase of the amount of the P(EO−EC)/$LiCF_3SO_3$ electrolyte, indicating that the Li-ions were more mobile. Correlation times, τ_c's, were calculated from the measured $T_{1\rho}$ values using the BPP equation. For the temperatures above T_{max}, which was the same temperature region where ionic conductivity measurements were carried out, correlation times, τ_c's, and activation energies, E_a's, for the polymer electrolytes gradually decreased with increase of the amount of the P(EO−EC)/$LiCF_3SO_3$ electrolyte. Thus, the Li-ion mobilities of a series of pore-filling polymer electrolytes depended on the P(EO−EC)/$LiCF_3SO_3$ electrolyte content at the same temperature range from 280 to 340 K and enhanced Li-ion mobilities led to the increase of ionic conductivity. From these results, it was therefore concluded that Li-ion mobilities were strongly correlated with ionic conductivities. So this polymer electrolyte based on a pore-filling system is expected to be a good candidate in rechargeable lithium batteries.

Acknowledgment. We are grateful to the Korea Science and Engineering Foundation (KOSEF) for support of this study through the Hyperstructured Organic Materials Research Center (HOMRC). S.-Y. Kwak gratefully acknowledges Professor Colin A. Fyfe at the Department of Chemistry, University of British Columbia (UBC) for his valuable suggestions and comments regarding the ^{7}Li solid-state NMR results during the author's sabbatical years at UBC.

References and Notes

(1) Meyer, W. H. *Adv. Mater.* **1998**, *10*, 439−448.
(2) Armand, M. *Solid State Ionics* **1994**, *69*, 309−319.
(3) Lightfoot, P.; Mehta, M. A.; Bruce, P. G. *J. Mater. Chem.* **1992**, *2*, 379−381.

(4) Nishimoto, A.; Agehara, K.; Furuya, N.; Watanabe, T.; Watanabe, M. *Macromolecules* **1999**, *32*, 1541−1548.
(5) Hall, P. G.; Davies, G. R.; Melntyre, J. E.; Ward, I. M.; Bannister, D. J.; Ie Brocq, K. M. F. *Polymer Commun.* **1986**, *27*, 98−100.
(6) Nicholas, C. V.; Wilson, D. J.; Booth, C.; Giles, J. R. M. *Br. Polym. J.* **1988**, *20*, 289−292.
(7) Chen-Yang, Y. W.; Hwang, J. J.; Huang, A. Y. *Macromolecules* **2000**, *33*, 1237−1244.
(8) Allcock, H. R.; Kuharcik, S. E.; Reed, C. S.; Napierala, M. E. *Macromolecules* **1996**, *29*, 3384−3389.
(9) Shi, Q.; Yu, M.; Zhou, X.; Yan, Y.; Wan, C. *J. Power Sources* **2002**, *103*, 286−292.
(10) Kim, D.-W.; Sun, Y.-K. *J. Power Sources* **2001**, *102*, 41−45.
(11) Michot, T.; Nishimoto, A.; Watanabe, M. *Electrochim. Acta* **2000**, *45*, 1347−1360.
(12) Jeon, J.-D.; Kwak, S.-Y.; Cho, B.-W. *J. Electrochem. Soc.* **2005**, *152*, A1583−A1589.
(13) Jeon, J.-D.; Cho, B.-W.; Kwak, S.-Y. *J. Power Sources* **2005**, *143*, 219−226.
(14) Xu, W.; Belieres, J.-P.; Angell, C. A. *Chem. Mater.* **2001**, *13*, 575−580.
(15) Forsyth, M.; Tipton, A. L.; Shriver, D. F.; Ratner, M. A.; MacFarlane, D. R. *Solid Sate Ionics* **1997**, *99*, 257−261.
(16) Kim, C. H.; Park, J. K.; Kim, W. J. *Solid State Ionics* **1999**, *116*, 53−61.
(17) Forsyth, M.; MacFarlane, D. R.; Meakin, P.; Smith, M. E.; Bastow, T. *Electrochim. Acta* **1995**, *40*, 2343−2347.
(18) Shan, W.; Zax, D. B. *Electrochim. Acta* **1997**, *42*, 3513−3518.
(19) Boudin, F.; Andrieu, X.; Jehoulet, C.; Oslen, I. I. *J. Power Sources* **1999**, *81*−*82*, 804−807.
(20) Every, H. A.; Zhou, F.; Forsyth, M.; MacFarlane, D. R. *Electrochim. Acta* **1998**, *43*, 1465−1469.
(21) Morales, E.; Acosta, J. L. *Electrochim. Acta* **1999**, *45*, 1049−1056.
(22) Kim, S. H.; Choi, J. K.; Bae, Y. C. *J. Appl. Polym. Sci.* **2001**, *81*, 948−956.
(23) Chung, S. H.; Jeffrey, K. R.; Stevens, J. R. *J. Chem. Phys.* **1991**, *94*, 1803−1811.
(24) Mello, N. C.; Bonagamba, T. J.; Panepucci, H.; Dahmouche, K.; Judeinstein, P.; Aegerter, M. A. *Macromolecules* **2000**, *33*, 1280−1288.
(25) Lin, C.-L.; Kao, H.-M.; Wu, R.-R.; Kuo, P.-L. *Macromolecules* **2002**, *35*, 3083−3096.
(26) Bloembergen, N.; Purcell, E. M.; Pound, R. V. *Phys. Rev.* **1948**, *73*, 679−712.
(27) Bishop, S. G.; Bray, P. J. *J. Chem. Phys.* **1968**, *48*, 1709−1717.
(28) Abragam, A. *Principles of Nuclear Magnetism*; Oxford Science Publications: Oxford, U.K., 1996.
(29) Kubo, R.; Tomita, K. *J. Phys. Soc. Jpn.* **1954**, *9*, 888−919.

MA061521V